INTERNATIONAL JOURNAL FOR NUMERICAL METHODS IN FLUIDS
Int. J. Numer. Meth. Fluids 2002; **38**:919–943 (DOI: 10.1002/fld.224)

Numerical simulation of flow in a circular duct fitted with air-jet vortex generators

Christoph Küpper*,† and Frank S. Henry

Department of Aeronautical, Civil and Mechanical Engineering, City University, Northampton Square, London, EC1V 0HB, U.K.

SUMMARY

Most of the fundamental studies of the use of air-jet vortex generators (AJVGs) have concentrated on their potential ability to inhibit boundary layer separation on aerofoils. However, AJVGs may be of use in controlling or enhancing certain features of internal duct flows. For example, they may be of use in controlling the boundary layer at the entrance to engine air intakes, or as a means of increasing mixing and heat transfer. The objective of this paper is to analyse the flow field in the proximity of an air-jet vortex generator array in a duct by using two local numerical models, i.e. a simple flat plate model and a more geometrically faithful sector model. The sector model mirrors the circular nature of the duct's cross-section and the centre line conditions on the upper boundary. The flow was assumed fully turbulent and was solved using the finite volume, Navier–Stokes Code CFX 4 (CFDS, AEA Technology, Harwell) on a non-orthogonal, body-fitted, grid using the k–ε turbulence model and standard wall functions. Streamwise, vertical and cross-stream velocity profiles, circulation and peak vorticity decay, peak vorticity paths in cross-stream and streamwise direction, cross-stream vorticity profiles and cross-stream wall shear stress distributions were predicted. Negligible difference in results was observed between the flat plate and the sector model, since the produced vortices were small relative to the duct diameter and close to the surface. The flow field was most enhanced, i.e. maximum thinning of the boundary layer, with a configuration of 30° pitch and 75° skew angle. No significant difference in results could be observed between co- and counter-rotating vortex arrays. Copyright © 2002 John Wiley & Sons, Ltd.

KEY WORDS: air-jet vortex generators; boundary-layer control; flow control; duct inlet

INTRODUCTION

Wallis [1, 2] seems to have been the first to achieve significant delay of flow separation of a turbulent boundary layer by employing circular air-jet vortex generators (AJVGs). AJVGs are created by forcing air through small orifices drilled through the solid surface at a pitch and skew angle to the on-coming flow. The interaction of the main flow and the issuing jet forms a longitudinal vortex in the streamwise direction. The longitudinal vortex is aligned

*Correspondence to: C. Küpper, Department of Meteorology, The University of Reading, Earley Gate, P.O. Box 243, Reading, RG66BB, U.K.
†E-mail: c.kupper@reading.ac.uk

Received 7 September 2000
Revised 27 January 2001

with the main flow and it induces mixing between the external or core stream and the boundary layer region. Thus, a redistribution of momentum within the boundary layer is promoted. Pearcey [3] applied the AJVG flow mixing technique to attenuate shock-induced flow separation on aerofoils. Several research groups have studied and analysed in more recent times the interaction of AJVGs with the main flow both experimentally and numerically. Johnston and Nishi [4], and Compton and Johnston [5] conducted experiments with AJVGs installed on a flat plate. Zhang [6], Henry and Pearcey [7] and Akanni and Henry [8] designed numerical models to simulate AJVG vortices on a flat plate. All groups reported that AJVGs had the potential for more advanced flow control than obtainable from the more conventional vane vortex generators.

Most of the fundamental studies of the use of AJVGs have considered external flows; i.e., boundary layer flows over aerodynamic surfaces. However, AJVGs may be of use in internal duct flows. For example, they have potential use as boundary layer control devices for engine air intakes (see Oskam and van der Berg [9]), or as a means of increasing mixing and heat transfer (see Jacobi and Shah [10]). The goal of the work presented in this paper was to investigate numerically the application of AJVGs to internal flows, and specifically their use as a means of controlling the boundary layer near the entrance of a straight circular intake duct. The geometry of the duct and AJVGs is based on that used by Gibb and Anderson [11].

NUMERICAL METHOD

Models

The numerical investigation was limited to the local area surrounding an array of 24 AJVGs, each of 1 mm in diameter, built into the wall of a straight circular duct of 128.8 mm in diameter (see Figure 1). The AJVGs were equi-spaced around the duct's circumference, and the array was located two diameters downstream of the duct inlet. Two basic AJVG configurations were simulated, i.e. co- and counter-rotating vortex arrays (see Figure 2). Co-rotating arrays comprise skewed AJVGs at the same angle to the on-coming flow. In a counter-rotating

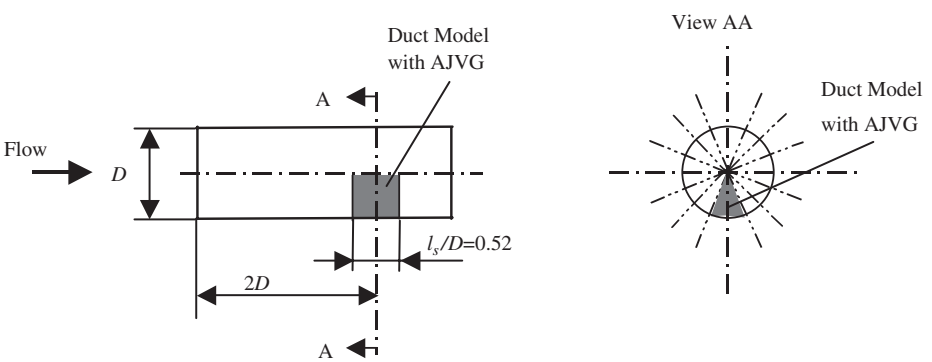

Figure 1. Circular duct with AJVG array.

configuration, each AJVG is skewed to the on-coming flow opposite in sign to its immediate neighbours. The difference between the two AJVG arrays in terms of the rotation sense and thus of the boundary conditions between the immediate neighbours can be clearly seen in Figure 2. In the co-rotating jet configuration, the boundaries between each pair of AJVGs can be described as a combination of upwash and downwash conditions. Conversely, in the counter-rotating configuration an alternating system of upwash and downwash conditions between two immediate vortex neighbours is generated.

Two numerical models were considered. These will be termed the sector model and the flat plate model (see Figure 3). The sector model describes the physical geometry and conditions of the flow field in the vicinity of the AJVGs within the duct more realistic than the flat plate model. Thus, the sector model is an optimized version of the previously designed simple flat plate model. In both cases, the jet inlet is centred on the lower surface of the solution domain. Figure 4 shows a plan view of the solution domain (grey shaded), which is applicable to both numerical models. In order to provide a computational efficient model the length is limited to exactly four times the width. The latter is fixed by the AJVG spacing. The relationship between the length parameters l_0 $(= l_{VG} - l_s/2)$, l_{VG} and l_s is demonstrated schematically in Figure 4 and all dimensions are listed in Table I.

The width of the sector model, w_s, was equal to the distance between each pair of the 24 AJVGs, i.e. $w_s = \pi D/24$. The width of the flat plate model was also set to $\pi D/24$. The lengths of both models were the same, i.e. $l_s = 4w_s$. However, the solution domain height, h_s, depended on the numerical model and was constant and equal to the radius, R, of the duct for the sector model. In contrast the solution domain height, h_s, of the flat plate model was defined as an integer multiple of the local undisturbed boundary layer thickness, δ, and hence increased with downstream distance. The local flat plate model height, h_s, was set to 5δ. The

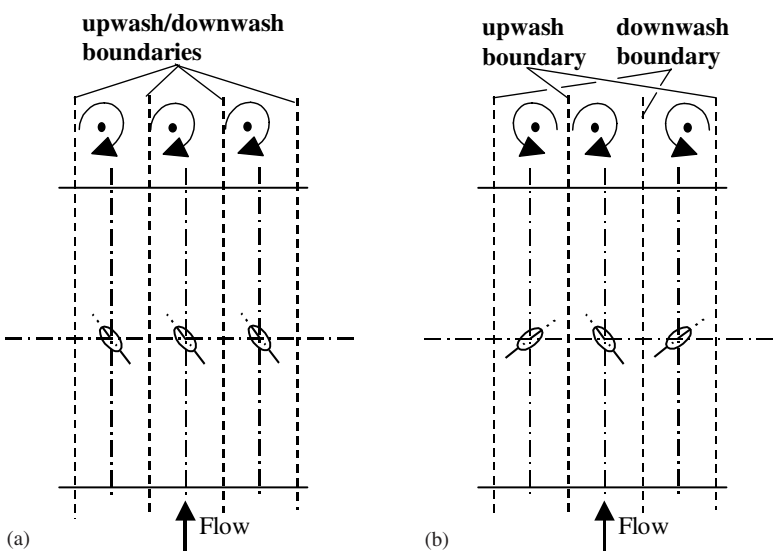

Figure 2. (a) Co- and (b) counter-rotating AJVG arrays.

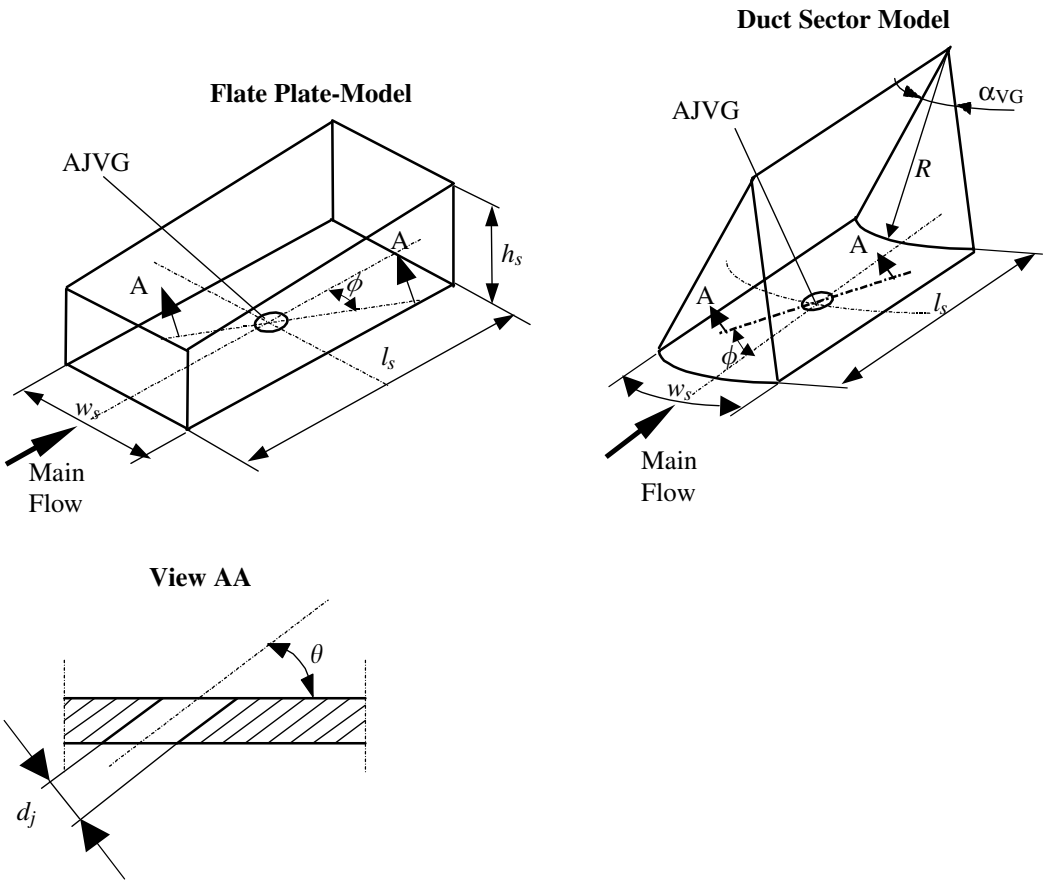

Figure 3. AJVG flat plate and sector model.

local boundary layer thickness was estimated using the correlation (see Schlichting [12]).

$$\delta = 0.37x\left(\frac{U_0 x}{v}\right)^{-0.2} \tag{1}$$

where the kinematic viscosity: $v = \mu/\rho$, and $\rho = 1.21\,\mathrm{kg\,m^{-3}}$ and $\mu = 1.81 \times 10^{-5}\,\mathrm{kg\,s^{-1}\,m^{-1}}$.

The CFD code CFX 4 (AEA Technology, Harwell) was used to solve the incompressible, steady, Reynolds-averaged Navier–Stokes equations. The k–ε model and standard wall functions were employed to model turbulence. It is recognized that the k–ε model together with the use of wall functions has been shown to have limitations. For instance, Henry and Reynolds [13] have shown analytically that for plane Couette flow the point at which the model equations are matched to the near wall boundary conditions is an important parameter of the numerical solution. However, while CFX 4 offers theoretically more precise models of turbulence these still rely on empirical correlations which have not yet been proved to apply

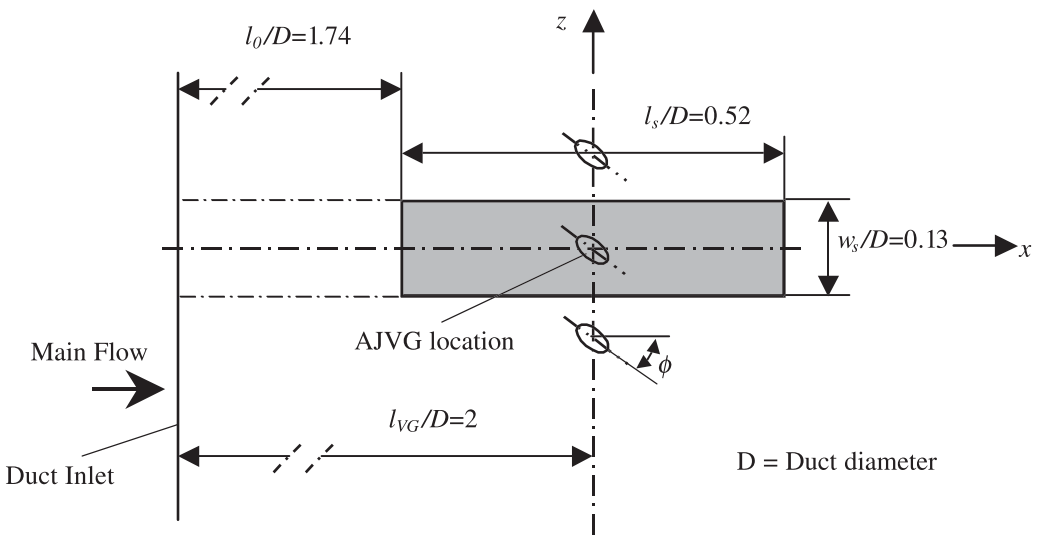

Figure 4. Co-rotating AJVG array with solution domain dimensions (grey shaded).

Table I. Details of the flat plate and sector AJVG models.

	Flat Plate Model	Sector Model
Duct diameter, D	0.1288 m	
Solution domain width, w_s	$\pi D/24 = 0.0169$ m $= 4\delta_0$	
Solution domain length, l_s	$4w_s = 0.0674$ m $= 17\delta_0$	
Solution domain height, h_s	5δ (see Equation (1))	$R = D/2 = 0.0644$ m
Pitch angle, θ	30°, 45° (see Figure 4)	
Skew angle, ϕ	30°, 45°, 60°, 75° (see Figure 4)	
Free stream velocity, U_0	254 m s^{-1}	
Airjet orifice diameter, d_j	0.001 m	
Jet velocity, U_j	U_0	
Distance between duct inlet and solution domain entrance, l_0	0.2239 m $= 55\delta_0$	
Inlet boundary layer height, δ_0	0.004 m (see Equation (1))	
Inlet Reynolds number, $Re_0 = \dfrac{\rho U_0 l_0}{\mu}$	3.8×10^6	

universally. Hence, it was felt that even with its known limitations the k–ε model offers the best compromise between accuracy and robustness.

The code is based on the finite volume method, and solves for pressure using the SIMPLEC pressure-correction method. A second-order higher upwind scheme was selected to model the advection terms. The equations were solved on a collocated, block-structured and body-fitted grid. An implementation of the Rhie–Chow algorithm for pressure–velocity coupling on collocated grids is used to avoid oscillations in the solution.

Boundary conditions

Solution domain inlet. The streamwise velocity profile at the solution domain inlet, u_s, was defined as a function of the y-direction (i.e. normal to the wall) only and in accordance with Prandtl's 1/7th power law (see Schlichting [12]). i.e.,

$$u_s = U_0 \left(\frac{y}{\delta_0} \right)^{1/7} \tag{2}$$

where δ_0 is the inlet boundary layer thickness calculated using Equation (1) and $x = l_0$. Both the vertical and cross-stream velocity components at the solution domain inlet were defined to be zero.

The turbulent kinetic energy, k_s, was estimated at the domain inlet using the experimentally determined correlation (see Hinze [14], p. 492)

$$k_s = \frac{-\overline{uv}}{0.32} \tag{3}$$

where the Reynolds stress, $-\overline{uv}$, in the boundary layer was estimated by

$$-\overline{uv} = \nu_t \left(\frac{\partial U}{\partial y} \right)$$

and the eddy viscosity, ν_t, was approximated according to Prandtl's mixing-length theory.

A state of local equilibrium within the boundary layer was assumed thus the dissipation rate of turbulence is approximately equal to the production rate of turbulence (see Hinze [14], p. 498). i.e.,

$$\varepsilon_s = -\overline{uv} \frac{\partial U}{\partial y} = \nu_t \left(\frac{\partial U}{\partial y} \right)^2 \tag{4}$$

Jet inlet. A plug profile was defined for the incoming jet velocity on the surface of the AJVG orifice. The magnitude of the AJVG inlet velocity, U_j, was defined to be a multiple of the free stream velocity U_0. In the computations discussed in this paper, U_j was set to be equal to U_0.

The turbulent kinetic energy, k_j, and the dissipation rate, ε_j, at the inlet of the jet were approximated by and taken from the CFX 4 Manual [15]:

$$k_j = 0.002 U_j^2 \tag{5}$$

$$\varepsilon_j = \frac{k_j^{3/2}}{0.3 d_j} \tag{6}$$

Küpper [16] and Küpper and Henry [17] studied the effect of the way in which the incoming jet flow is modelled on the resulting downstream flow by computing both the flow in the inlet tube and at the jet inlet. The conclusion was that no essential difference of the downstream development of the vortex could be observed. Thus, the plug profile is believed to be an appropriate description of the jet flow at the AJVG inlet.

The outlet boundaries were set to constant pressure. The side boundaries were set either symmetric (array of counter-rotating vortices) or periodic (array of co-rotating vortices).

The upper boundaries were differently defined for the two numerical models. In the case of the flat plate model, the upper boundary imposed was set to constant pressure. The sector model's upper boundary represents the centre line of the duct and hence it was set to be axis-symmetric.

Grid and numerical solution. A FORTRAN routine was written to generate a non-orthogonal, block-structured grid with 13 blocks in an algebraic manner. The only difference between the two numerical models is the coordinate system employed. The Cartesian coordinate system was used for the flat plate model whereas the polar coordinate system was employed for the sector model. An isometric view of the meshes can be seen in Figure 5. A plan view of the two grids and a detailed view of the inner block configuration are shown in Figure 6.

Grid independence was judged by the wall shear stress distribution over a reference cross plane. The number of grid points normal to the wall were calculated by ensuring that y^+ was in the range of $30 \leqslant y^+ \leqslant 100$ (see Rodi [18]). The skin friction distribution was observed to be insensitive to further grid refinement for a mesh of 89 088 cells for the flat plate model, and 119 964 cells for the sector model. Küpper [16] investigated a variety of advection schemes (see CFX 4 Manual [15]) by comparing predicted velocity profiles to experimental data. The result showed that the second-order higher upwind (HUW) advection scheme (see CFX 4 Manual [15]) offered the best overall performance. Küpper [16] and Küpper and Henry [17] also compared predicted results with experimental data and showed reasonably good agreement between the predicted and measured data. However, the predicted vortex was weaker than the

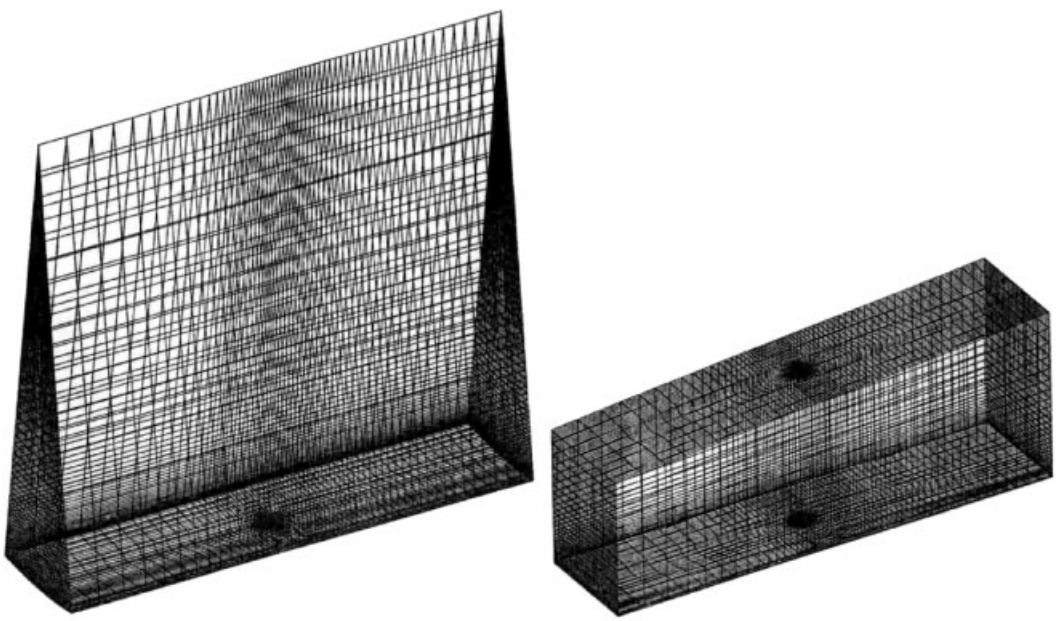

Figure 5. Isometric view of the numerical grids of the Sector and Flat Plate Model.

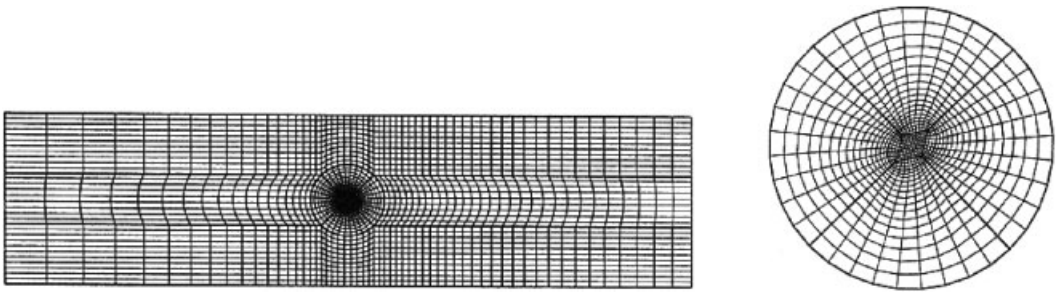

Figure 6. View of the AJVG grids in the (x–z) plane and detailed view of the inner block configuration.

measured one. Convergence was typically achieved after 1000 iterations for the flat plate model and 2500 iterations for the sector model. The mass source residual, i.e. the error in continuity, was reduced by an average reduction factor of approximately 10^5.

RESULTS

The numerical predictions of the three velocity components, the vorticity profiles, and the wall shear stress are presented at two downstream planes. The decay of circulation and peak vorticity in the streamwise direction and the peak vorticity paths are presented. The reference locations, $x_1 = 0.25 l_s$ (4.2 δ_0) and $x_2 = 0.46 l_s$ (7.7 δ_0), are shown schematically in Figure 7.

Figure 8 show velocity vector plots predicted by the sector model at the two reference planes. The array of counter-rotating vortices migrates to the side, as potential theory predicts, and decay in streamwise direction.

Streamwise, vertical and cross-stream velocity profiles are given in Figures 9, 10 and 11, respectively, at the two downstream locations, x_1 and x_2. All profiles are passing through the vortex cores. No differences between the predictions of streamwise velocities produced by co- and counter-rotating vortices for each AJVG model can be seen at location x_1 and only minor differences are seen at location x_2. The streamwise velocity deficits (see Figure 9) at x_1 and the magnitude of the vertical velocity profiles (see Figure 10) at x_1 and x_2 predicted by the sector model were approximately 7 per cent less than those predicted by the flat plate model. The cross-stream positions of the vortices at x_1 and x_2 produced by both models are approximately identical.

In Figure 11 the cross-stream velocity profiles indicate identical vertical positions of all vortices predicted by both models at the downstream location x_1. The vertical vortex centre positions are where the velocity profiles cross the y-axis. Between x_1 and x_2 the co-rotating vortex cores predicted by the sector model rose by approximately 30 per cent whereas the flat plate model predicted a rise of approximately 25 per cent. The predicted cross-stream velocities of the sector model close to the wall are again 7 per cent less than those of the flat plate model at both downstream locations, x_1 and x_2. Slightly higher velocity magnitudes can be observed for the co-rotating vortices compared to the counter-rotating vortices close to the wall for both models and at both locations, x_1 and x_2. Conversely, the velocity magnitudes above the vortex cores were slightly higher for the counter-rotating than for the co-rotating vortices. At both downstream locations, the cross-stream velocity profiles coincide up to the

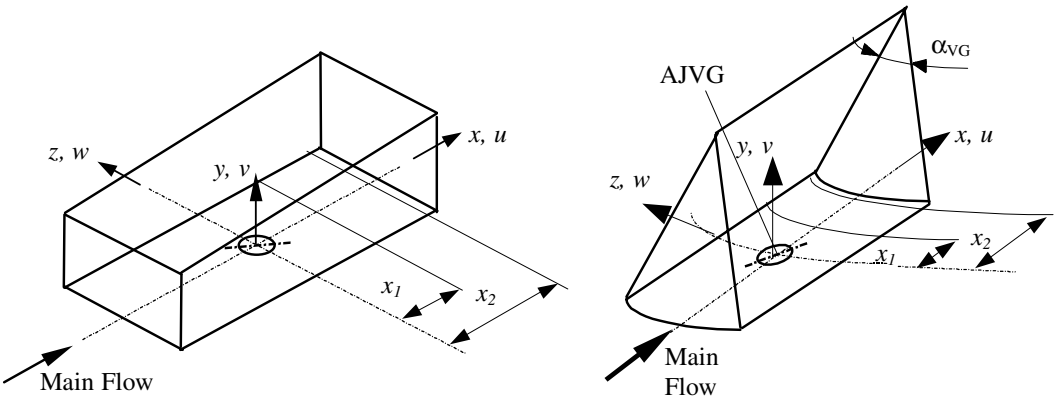

Figure 7. Schematic of the AJVG models with the two downstream locations, x_1 and x_2.

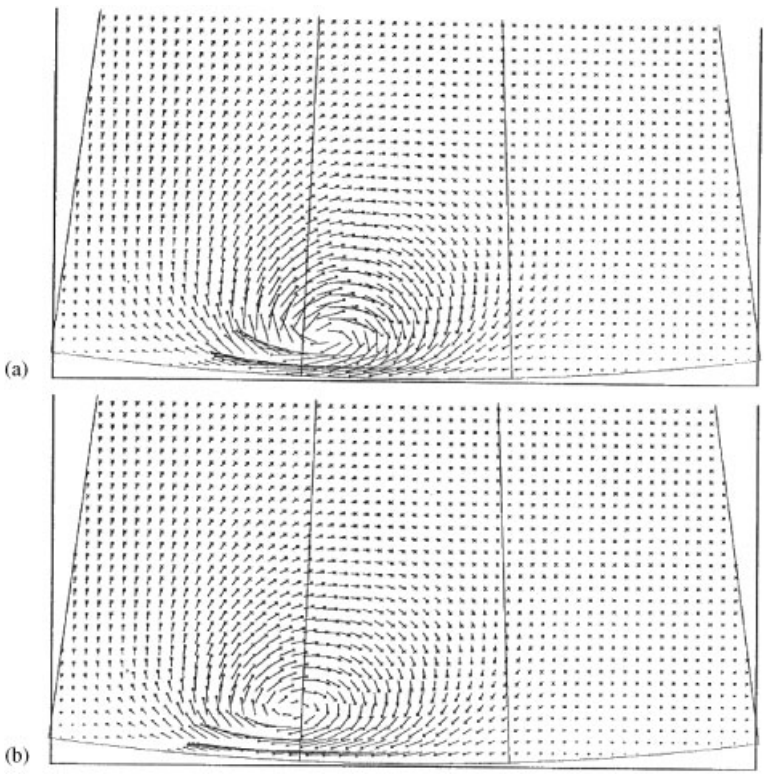

Figure 8. Velocity vector plots of the counter-rotating vortices of pitch/skew angle of 45°/45° at the reference planes, (a) $x_1 = 0.25l_s$ (4.2 δ_0) and (b) $x_2 = 0.46l_s$ (7.7 δ_0).

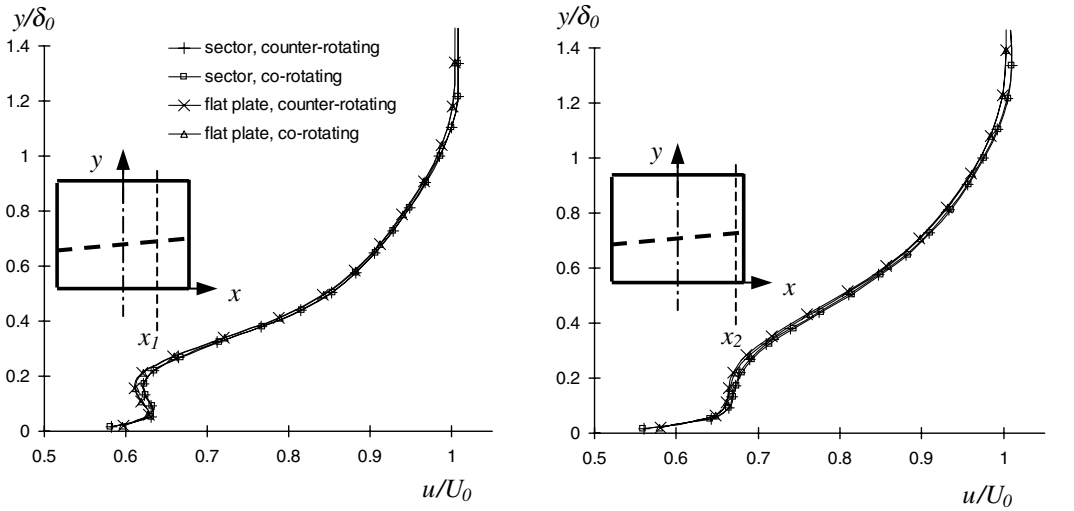

Figure 9. Streamwise velocity profiles through the vortex cores for the sector and flat plate models with 45° pitch and 45° skew angle at two downstream planes, x_1 and x_2.

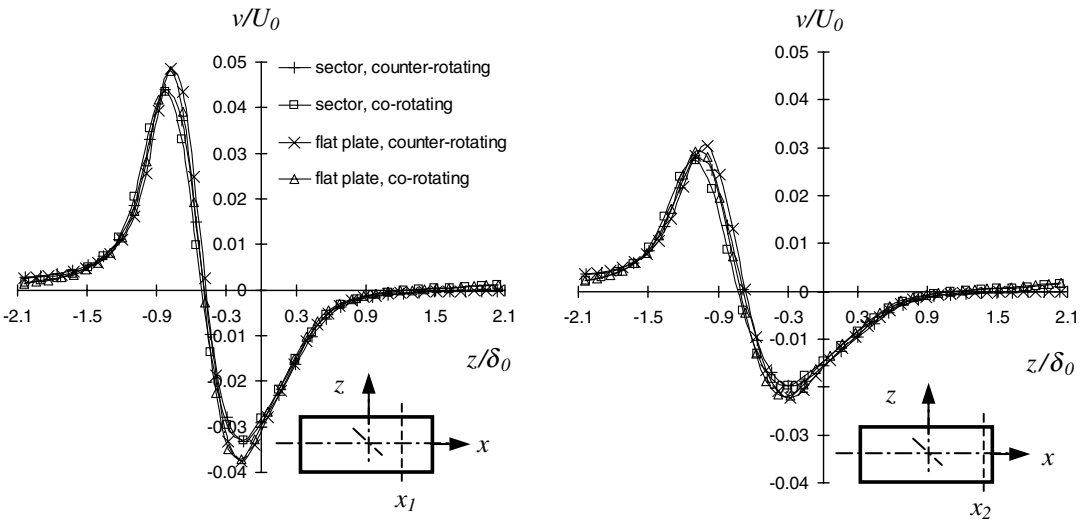

Figure 10. Vertical velocity profiles through the vortex cores for the sector and flat plate models with 45° pitch and 45° skew angle at two downstream planes, x_1 and x_2.

vortex core positions and diverge slightly towards the negative velocity maxima. At location x_1 the co-rotating vortices of the sector model shows the lowest negative velocity maximum whereas the counter-rotating vortices produced by the flat plate model generated the highest negative velocity maximum. Identical profiles of the negative velocity maxima were produced by counter-rotating vortices of the sector model and co-rotating vortex arrays of the flat plate

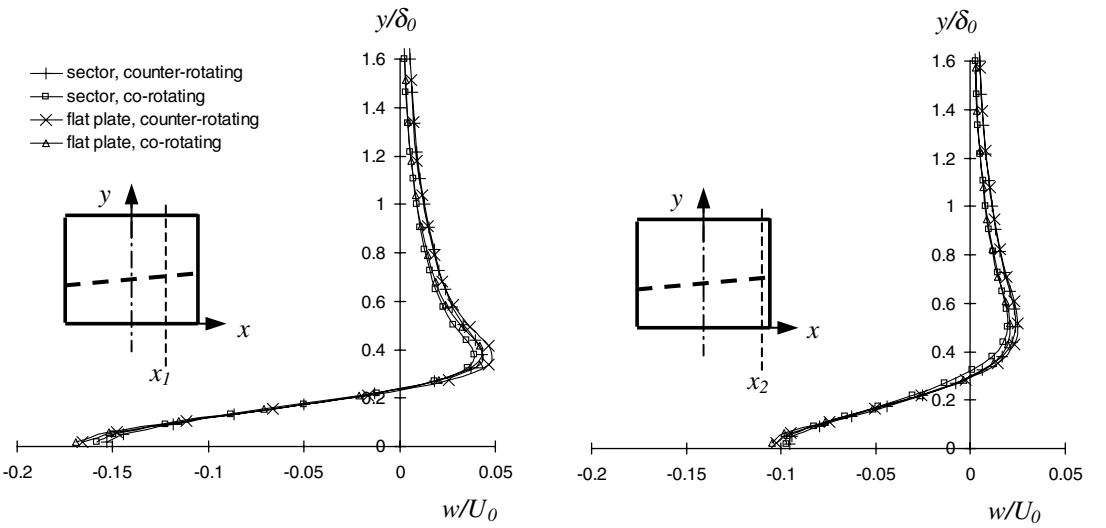

Figure 11. Cross-stream velocity profiles through the vortex cores for the sector and flat plate models with 45° pitch and 45° skew angle at two downstream planes, x_1 and x_2.

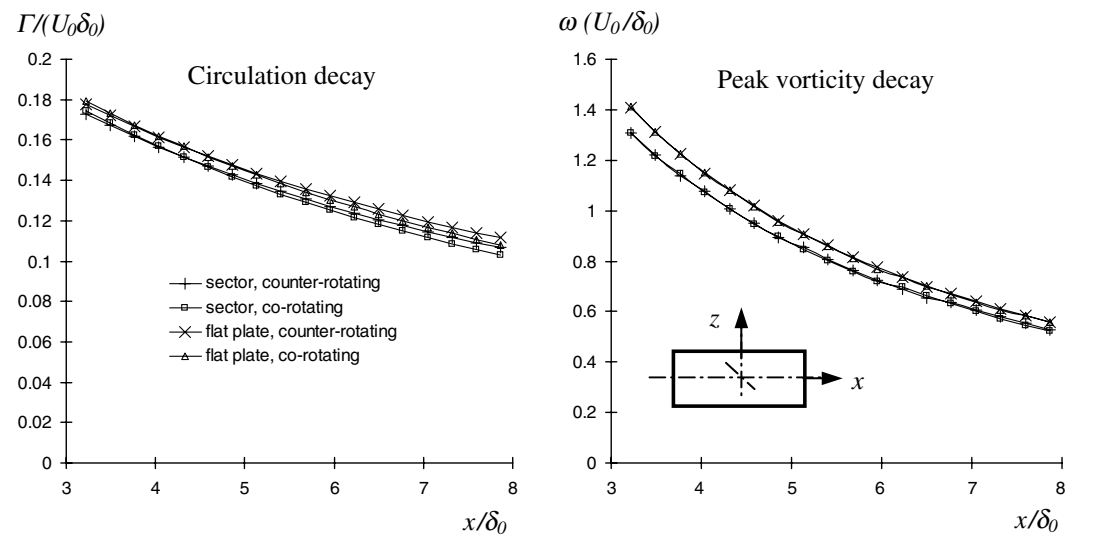

Figure 12. Circulation and peak vorticity decay for the sector and flat plate models with 45° pitch and 45° skew angle.

model at location x_1. Above the location of the negative velocity maxima at x_1 and from the location of the negative velocity maxima at x_2 the two jet models describe identical results.

Figure 12 shows the circulation and peak vorticity decay in the streamwise direction. The magnitudes of circulation of the sector model are approximately 2 per cent less than those of

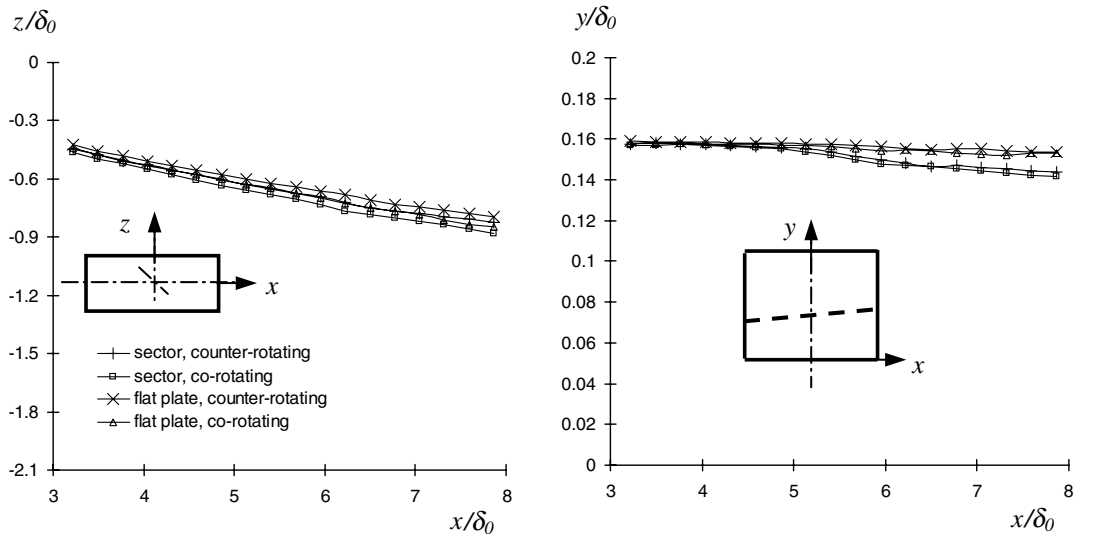

Figure 13. Peak vorticity paths for the sector and flat plate models with 45° pitch and 45° skew angle in the x–z and x–y plane.

the flat plate whereas the decay rate of both models is equal. The decay rates of circulation were seen to differ equally for each jet model depending on the rotational sense of the vortices. Through interference of neighbouring vortices the circulation of the co-rotating configuration decayed slightly faster than in the case of counter-rotating vortex arrays. The magnitudes of peak vorticity of the sector model is initially approximately 7 per cent less than that of the flat plate model but decreases to approximately 2 per cent at the solution domain end. In the streamwise direction, the decay rate of peak vorticity of the sector model is also slightly less than in the case of the flat plate model. No difference in peak vorticity decay between the co- and counter-rotating vortices of each model can be observed.

Figure 13 demonstrates the paths of peak vorticity in streamwise direction looking onto the solution domain (plan view/left panel) and from the side (side view/right panel). Hence, the movement of the vortices in the cross-stream and vertical directions can be observed. The counter-rotating vortex of the flat plate model describes the closest path to the solution domain centre line (left panel), i.e. where the z-coordinate is zero. The next adjacent path is described identically by the co-rotating vortex of the flat plate and the counter-rotating vortex of the sector model. The co-rotating vortex of the sector model describes the third path. The difference between the peak vorticity paths of the co- and counter-rotating vortices generated by each of both jet models is less than 1 per cent. A divergence of the peak vorticity paths predicted by the two jet models occurs in the x–y plane (see Figure 13, right panel) from a downstream location of approximately $x/\delta_0 = 5$. The sector model vortex paths approach closer to the wall than those produced by the flat plate model. However, the difference in heights of the paths is negligible compared to the distances travelled by the vortices in the cross-stream direction. The total distance moved in the y-direction is only 2 per cent of the distance travelled downstream whereas the vor-

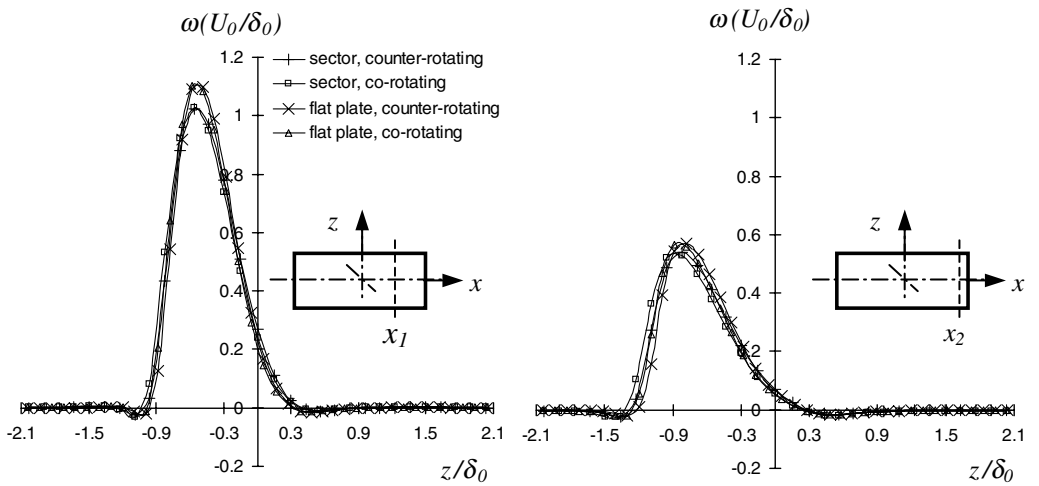

Figure 14. Cross-stream vorticity distribution through the vortex cores for the sector and flat plate models with 45° pitch and 45° skew angle at two downstream planes, x_1 and x_2.

tices travelled approximately 40 per cent of the total downstream path in the cross-stream direction.

Figure 14 describes the cross-stream vorticity distribution through the vortex cores at the downstream planes, x_1 and x_2. Again, the sector model predictions of peak vorticity at location x_1 are approximately 7 per cent less than those of the flat plate model. The difference in cross-stream vorticity distribution between the two jet models vanishes further downstream at the location x_2. No significant secondary or negative vorticity (see Pauley and Eaton [19]) can be observed for either model.

Figure 15 shows the vorticity profiles through the vortex cores at x_1 and x_2. Similar results can be observed as seen in Figure 14. That is, the sector model predictions of peak vorticity at location x_1 are approximately 7 per cent lower than those of the flat plate model. The difference in the magnitudes of the vorticity profiles between the two jet models decreased to approximately 3 per cent at the location x_2.

Figure 16 presents the skin friction distribution in the cross-stream direction at x_1 and x_2. No significant differences between the shear stress predictions of the two models can be observed.

Figures 17 to 27 are shown to discuss various configurations of pitch and skew angles of the AJVG for the local duct sector model. All figures describe either the distribution of a particular parameter along the x-axis, i.e. in streamwise direction or at one reference downstream plane (see Figure 7), i.e. at $x_1 = 0.25 l_s$ (4.2 δ_0). Figures 17 to 19 comprise the streamwise, vertical and cross-stream velocity profiles passing through the vortex cores. As observed in Figures 9 to 16, there are only small differences between co- and counter-rotating vortices generated by the jet.

Careful inspection of Figure 17 shows that the velocity gradient from the solid surface to the inflection point of the streamwise velocity profiles depends very much on the value of the skew angle. Each angle configuration with high skew ($\phi \geqslant 60°$) produced very steep velocity

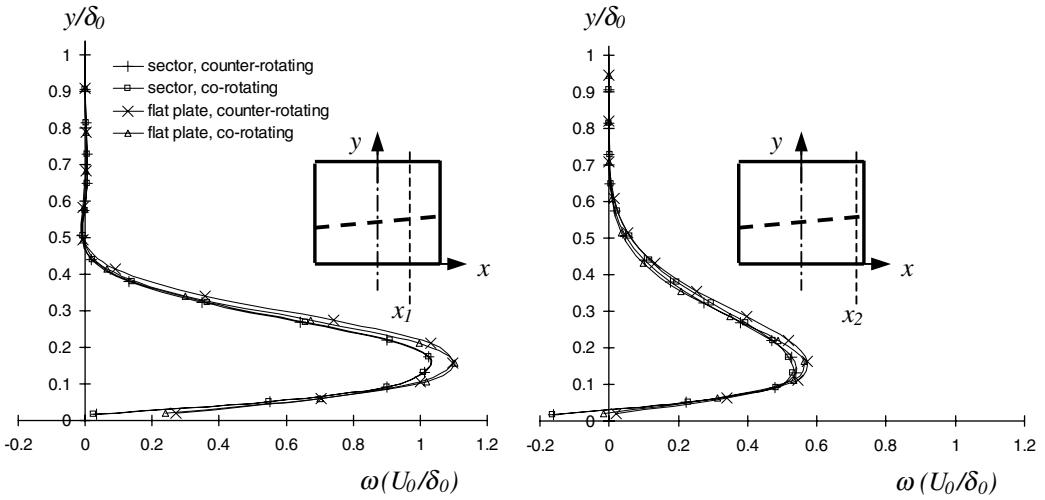

Figure 15. Vorticity profiles through vortex cores for the sector and flat plate models with 45° pitch and 45° skew angle at two downstream planes, x_1 and x_2.

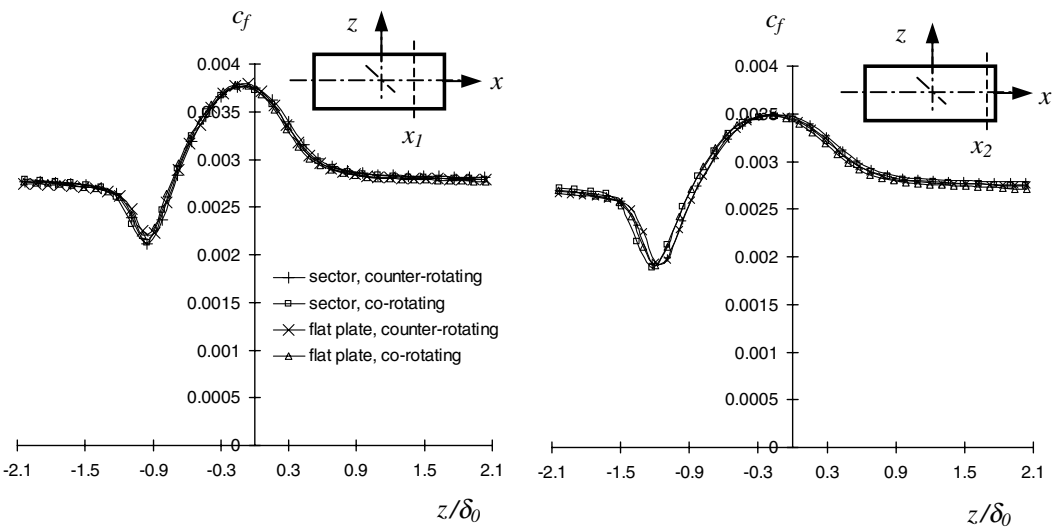

Figure 16. Cross-stream wall shear stress distribution for the sector and flat plate models with 45° pitch and 45° skew angle at two downstream planes, x_1 and x_2.

gradients between the first and second data point above the wall. These velocity profiles also have lower magnitudes at the first inflection point. The pitch/skew configuration of 45°/75° described the profile with the lowest magnitude whereas the case of 30°/30° predicted the highest velocity magnitude and the biggest velocity difference between the first and second

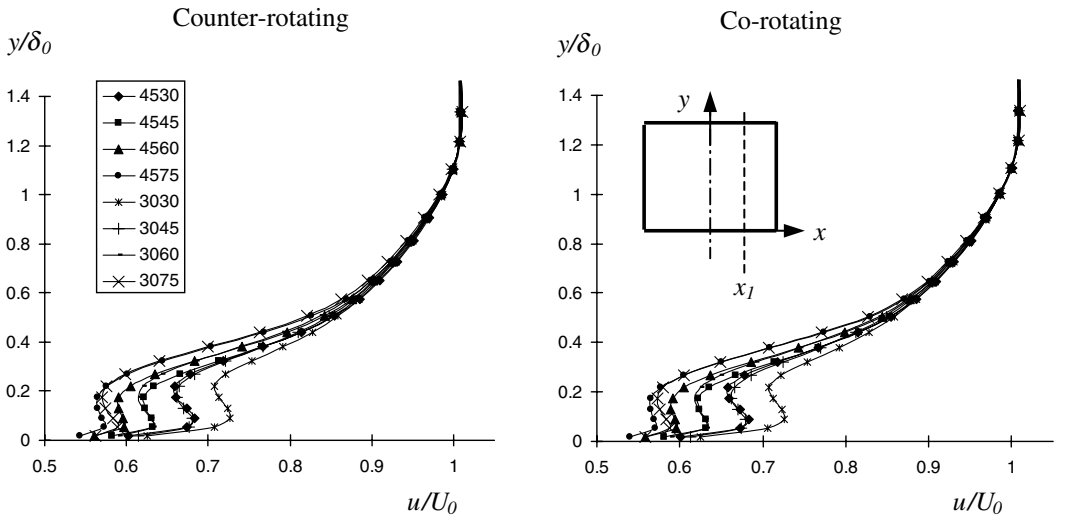

Figure 17. Streamwise velocity profiles through the vortex cores for various pitch/skew angle configurations of the AJVG at the downstream plane x_1.

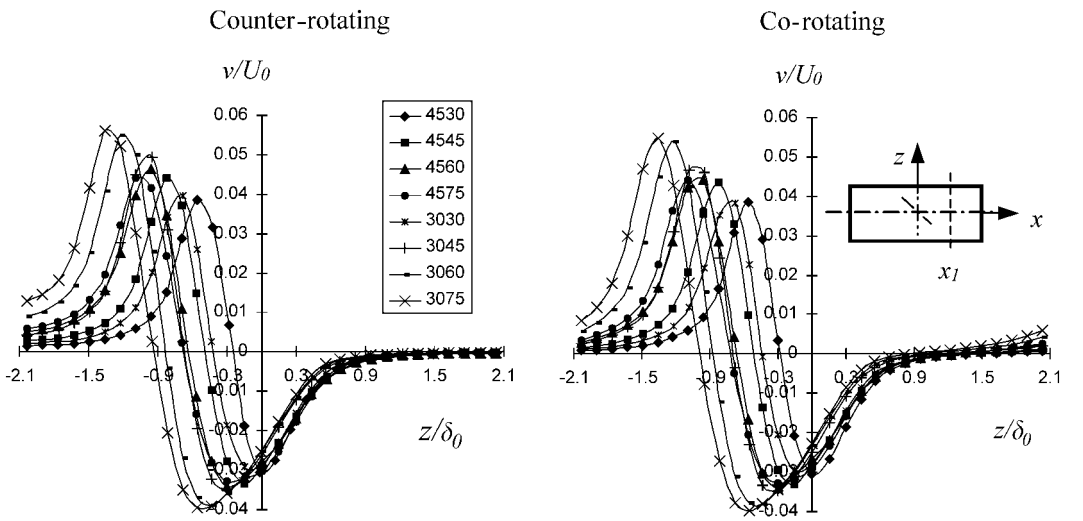

Figure 18. Vertical velocity profiles through the vortex cores for various pitch/skew angle configurations of the AJVG at the downstream plane x_1.

data point. An overall smooth return to free stream conditions with increasing boundary layer thickness can be observed.

In Figure 18 the vertical velocity profiles at the reference plane x_1 exhibit a small difference between the co- and counter-rotating vortices. Especially for high skew angles, i.e. $\phi \geqslant 60°$, the periodicity of the co-rotating vortices can be observed. The jet configurations with pitch/skew

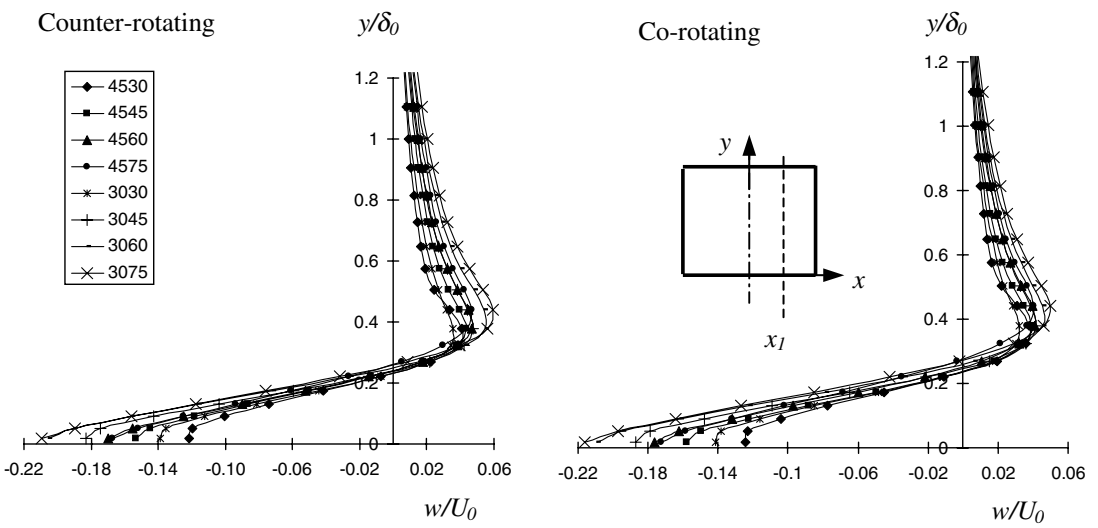

Figure 19. Cross-stream velocity profiles through the vortex cores for various pitch/skew angle configurations of the AJVG at the downstream plane x_1.

angles of 30°/75° and 30°/60° produced the strongest vertical velocities while configurations of 45°/30° and 30°/30° initiated the weakest vertical velocity magnitudes.

The cross-stream velocity profiles in Figure 19 support the previous findings of Figure 18. Hence, the two configurations of 30°/75° and 30°/60° produced the highest magnitudes whereas the configurations of 45°/30° and 30°/30° provided the lowest magnitudes. The counter-rotating vortices show slightly stronger cross-stream velocity components above their cores whereas the co-rotating vortices exhibit higher velocity magnitudes below their cores. Even though all vortices described approximately the same distance from the wall, the counter-rotating vortices spread slightly more into the free stream above the boundary layer than the co-rotating vortices.

In Figure 20, the highest levels of circulation downstream of the jet were produced by the pitch/skew angle configurations of 30°/75° and 30°/60°. The third, fourth and fifth highest initial magnitude of circulation was achieved by angle configurations of 45°/75°, 45°/60° and 30°/45°, respectively. However, all three configurations decayed approximately to a single value at the solution domain end. The lowest production of circulation was generated by the angle pairs of 45°/45°, 30°/30° and 45°/30°. The initial level of circulation could be increased by a factor of approximately 2.8 and the final level of circulation could also be increased by a factor of approximately 2.2 by changing the pitch/skew angle configuration from 45°/30° to 30°/75°.

Figure 21 shows the peak vorticity decay and reveals the same effect of pitch/skew angle configurations as observed for circulation. Even though the difference between the angle configuration is not as distinguishable as it was for circulation, the highest and lowest level of peak vorticity can be clearly seen at 30°/75° and 45°/30°, respectively. The factor between the highest and the lowest peak vorticity is approximately 1.3 compared to 2.8 for the circulation. The peak vorticity decay can be described to be similar to an exponential function where all

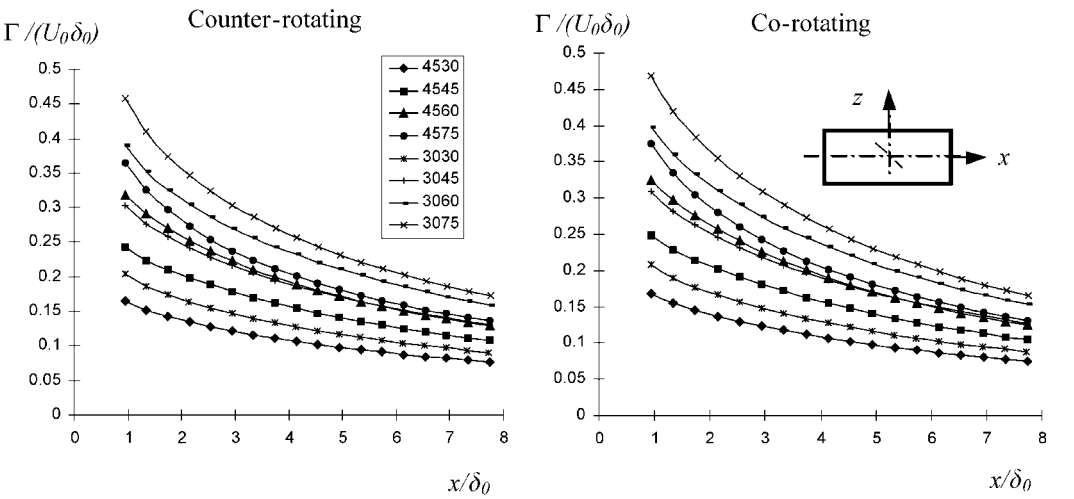

Figure 20. Circulation decay for various pitch/skew angle configurations of the AJVG.

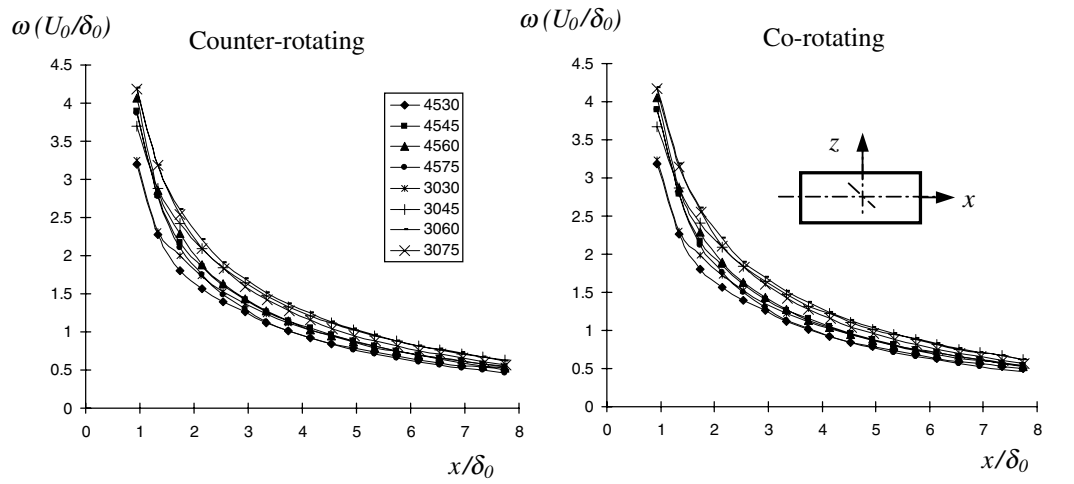

Figure 21. Peak vorticity decay for various pitch/skew angle configurations of the AJVG.

pitch/skew angle configurations reach approximately the same level at the solution domain exit.

Figures 22 and 23 describe the peak vorticity paths from two different perspectives. Figure 22 exhibits a plan view onto the wall, thus, the locus of peak vorticity can be seen as a projection on the x–z plane. In contrast, in Figure 23 a side view of the locus of peak vorticity is shown, i.e. paths of peak vorticity projected on the x–y plane.

In Figure 22 there are two groups of angle configurations, (1) 30°/75° and 30°/60° and (2) 30°/30° and 45°/30° which describe the longest and the shortest distances travelled from the centre line of the solution domain to the upwash (see Figure 2) domain boundary. These

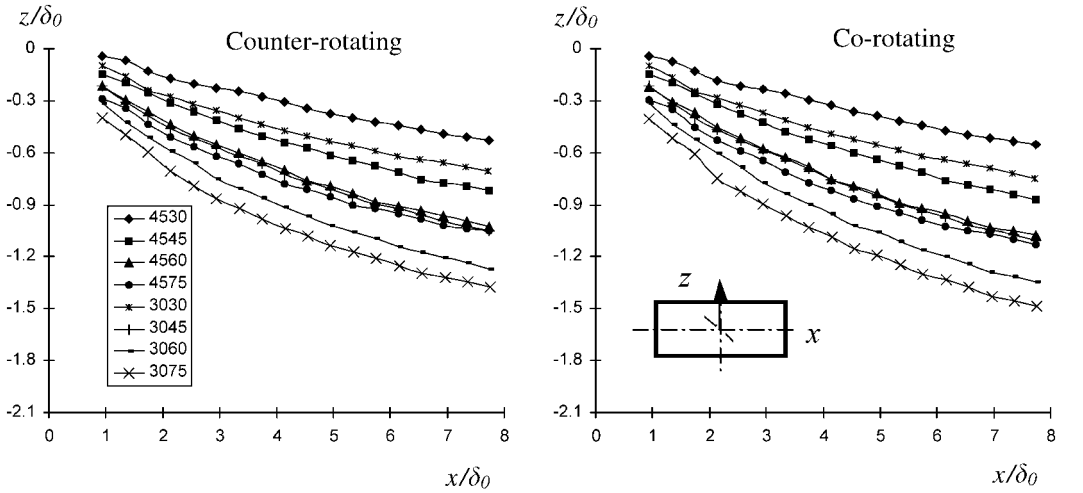

Figure 22. Peak vorticity paths for various pitch/skew angle configurations of the AJVG in the x–z plane.

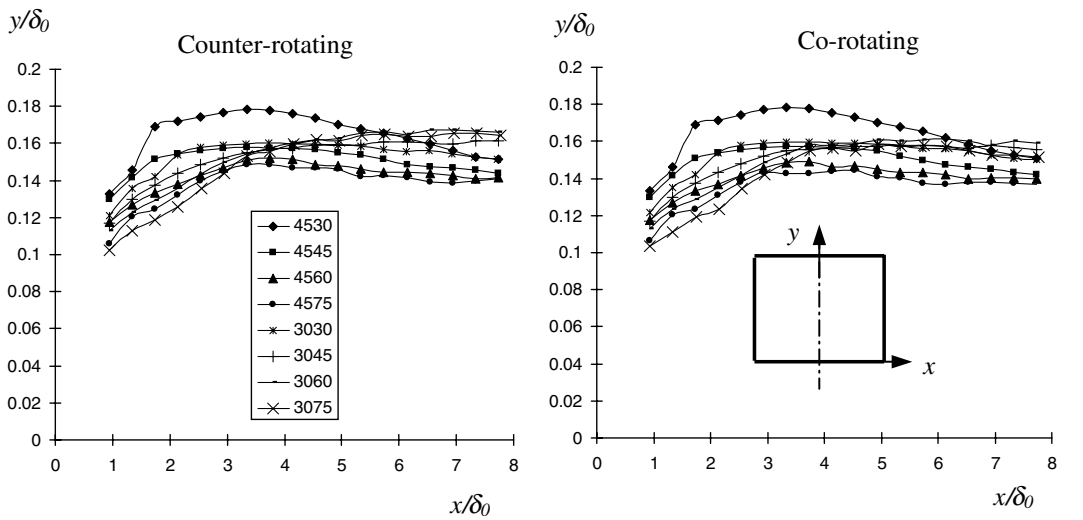

Figure 23. Peak vorticity paths for various pitch/skew angle configurations of the AJVG in the x–y plane.

two groups generated the highest and lowest level of circulation and peak vorticity as seen in Figures 20 and 21. The configurations of 45°/60°, 30°/45° and 45°/75° travelled on similar paths. At the first downstream location, the angle pairs 45°/75° and 30°/60° coincide initially but diverge further downstream.

Figure 23 reveals that the two angle configurations 30°/75° and 30°/60° describe the most monotonically ascending peak vorticity paths. Those configurations produced also the highest

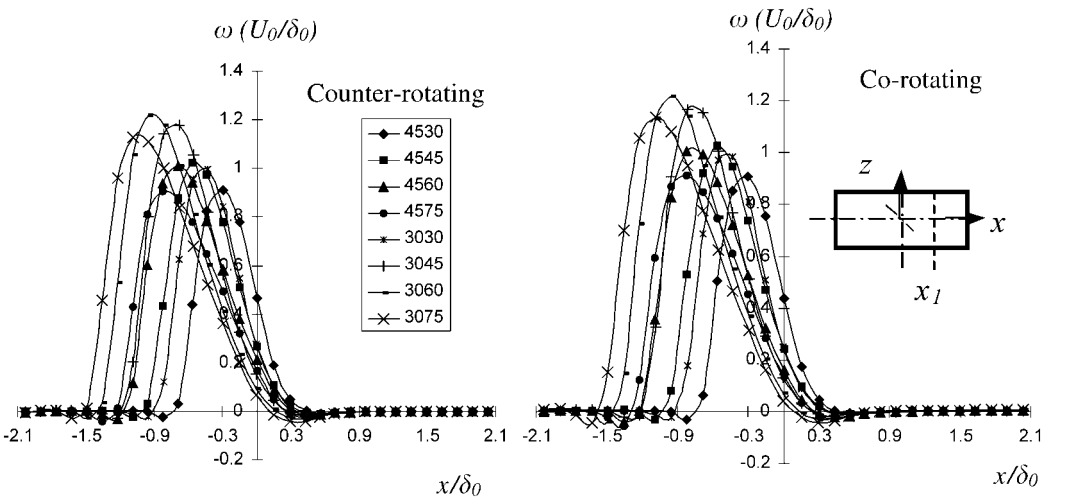

Figure 24. Cross-stream vorticity distribution through the vortex cores for various pitch/skew angle configurations of the AJVG at the downstream plane x_1.

level of circulation (see Figure 20). The peak vorticity paths of these two angle configurations rose by approximately 66 per cent from their initial positions to an approximate downstream location of $x/\delta_0 = 5.5$. From that location further downstream, the vortices of the angle configurations 30°/75° and 30°/60° travelled approximately on horizontal paths. With the exception of the 45°/30° configuration and the two described above, all remaining configurations predicted peak vorticity paths that rose by approximately 20 to 40 per cent from their initial position to a downstream location of $x/\delta_0 = 5.5$. They continued a path further downstream slightly towards the wall. The case of 45°/30° produced peak vorticity paths that rose rapidly about approximately 30 per cent from the initial position to a downstream location of $x/\delta_0 = 2$ and continued travelling back towards the wall. The final position was approximately 14 per cent further away from the wall than the initial. It is important to emphasize that the y-axis is greatly magnified, i.e. the peak value of the y-axis is only 2.5 per cent of the total downstream length of the solution domain. Hence, the distance travelled from and towards the wall is negligible compared to the distance travelled in cross-stream direction.

In Figure 24 the cross-stream vorticity distribution through the vortex cores is shown at the downstream location x_1. Taking the assumption that the area beneath the vorticity profiles represents the magnitudes of vorticity distribution, again the two angle configurations, 30°/75° and 30°/60° predicted the highest level of vorticity. Small magnitudes of negative or secondary vorticity can be seen for all predictions.

In Figure 25 vorticity profiles through the vortex cores are shown and only for the angle configuration of 45°/30° can negative vorticity be observed. The maximum amplitude of vorticity can be seen for the configuration of 30°/60° and the smallest amplitudes for the configurations of 45°/30° and 45°/75°.

Figure 26 shows the cross-stream wall shear stress distribution at the downstream reference plane x_1. The highest level of skin friction enhancement was achieved by using the pitch/skew

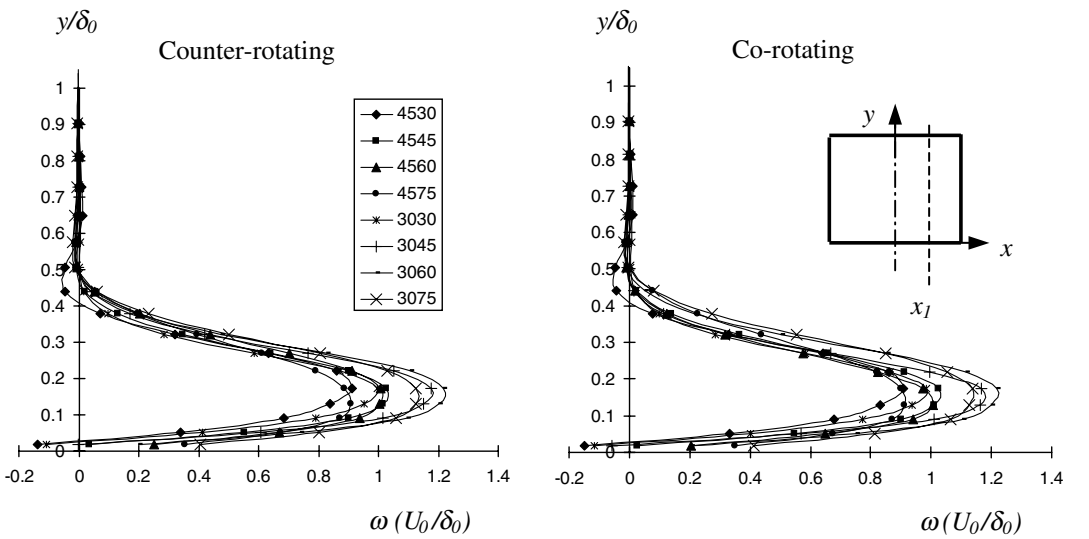

Figure 25. Vorticity profiles through vortex cores for various pitch/skew angle configurations of the AJVG at the downstream plane x_1.

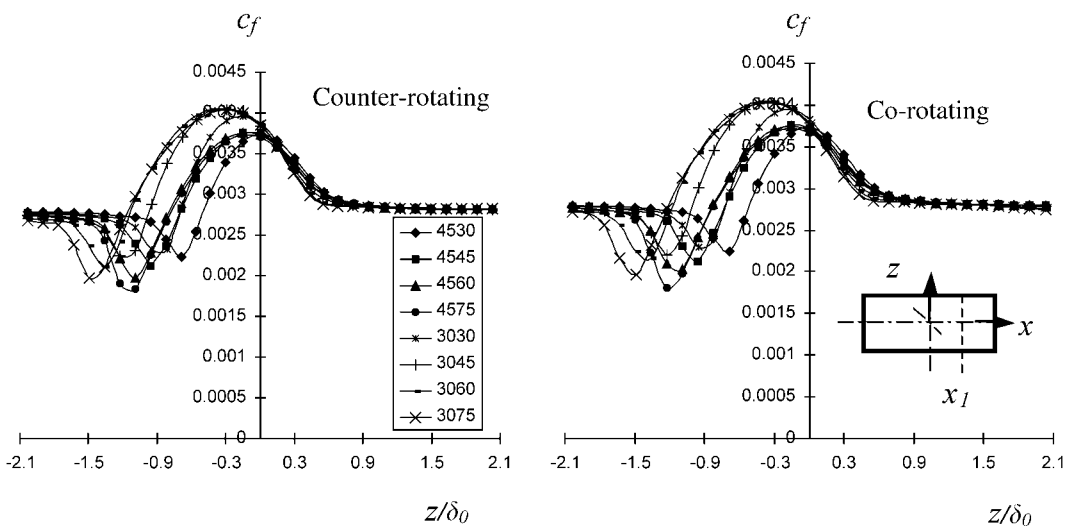

Figure 26. Cross-stream wall shear stress distribution for various pitch/skew angle configurations of the AJVG at the downstream plane x_1.

angle configurations of 30°/75° and 30°/60° whereas the lowest enhancement was predicted by the configuration of 45°/30°. A small difference between the co- and counter-rotating vortices can be observed. However, the difference is only visible for the cases of 30°/75° and 30°/60°.

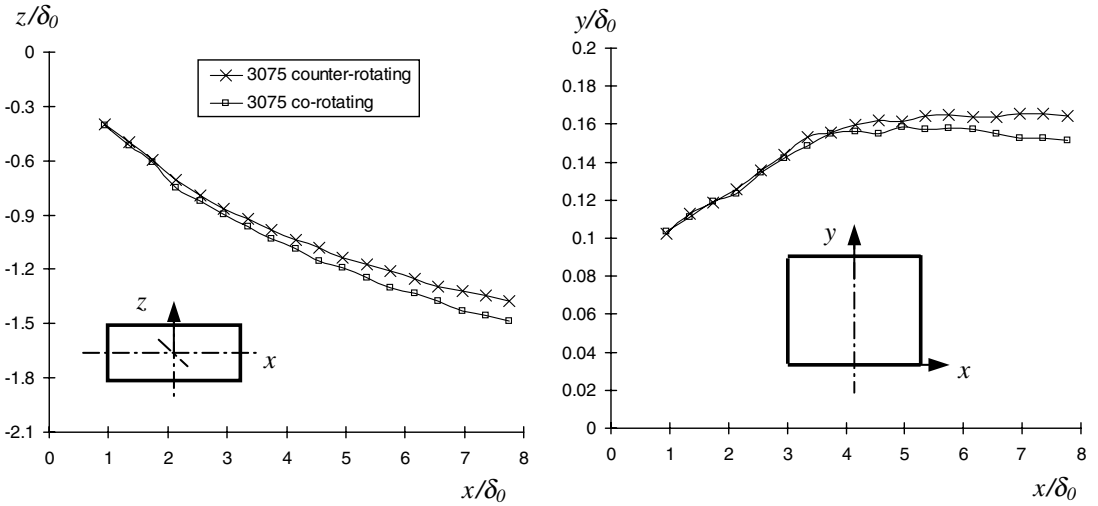

Figure 27. Peak vorticity paths for the AJVG with 30° pitch and 75° skew angle.

Peak vorticity paths of the co- and counter-rotating vortices of the pitch/skew angle configuration of 30°/75° are given in Figure 27. This configuration was chosen because it predicted the highest level of circulation, peak vorticity and increase of skin friction. This figure is given to illustrate on one graph co- and counter-rotating vortex configurations. As observed before, the difference between the prediction of co- and counter-rotating vortices is very small. The co-rotating vortices experience slightly more translation in the cross-stream direction than the counter-rotating vortices onwards from a downstream location of $x/\delta_0 \approx 2$. The difference in height, shown on the right panel of Figure 27 is negligible because the peak value of the y-axis is only 2.5 per cent of the total downstream length of the solution domain.

DISCUSSION

It has been shown that the magnitudes of the sector model results were in general marginally smaller (7 to 2 per cent) than those of the flat plate model with the exception of wall shear stress distribution (see Figure 16). The enhancement of skin friction was predicted to be the same using either the sector or the flat plate model. Little difference between the results for co- and counter-rotating vortices for each of the AJVG models was observed. The sector model predictions of streamwise velocity deficits (see Figure 9) at the first downstream location, x_1, vertical velocity profiles and cross-stream velocities close to the wall (see Figures 10 and 11) at both downstream locations (x_1 and x_2), magnitudes of peak vorticity (see Figure 12), level of cross-stream vorticity and magnitudes of vorticity profiles (see Figures 14 and 15) at location x_1 were all slightly lower (~ 7 per cent) than those for the flat plate model. The difference in magnitudes of vorticity profiles decreased to 3 per cent and of peak vorticity to 2 per cent from the first (x_1) to the second reference plane (x_2). The prediction of circulation

(see Figure 12) of the sector model was only 2 per cent lower than that of the flat plate model, but the decay rate of circulation of the two models were identical. The vortices predicted by the sector model lifted of the wall approximately 5 per cent more than those produced by the flat plate model (see Figure 11). The cross-stream peak vorticity paths (see Figure 13) predicted by the two numerical models differed by less than 1 per cent.

According to the presented results, it can be clearly seen that no significant differences in flow field predictions were obtained using the sector as opposed to the flat plate model. It is believed that the position and strength of the produced vortex arrays play an important role in the magnitude of different results between the two numerical models. An inspection of Figure 8 shows that the vortex is relatively weak and close to the wall. A comparison of the general results between co- and counter-rotating vortices (Figures 9 to 16) reveals that there is no relevant interaction between neighbouring vortices. Hence, the cross-stream curvature and the different height of the upper boundary of the sector model compared to the flat plate model did not exhibit any significant influence on the development of the vortices. In the sector model the upper boundary is equal to the symmetry line of the duct whereas the flat plate model has a downstream increasing solution domain height of five times the local boundary layer thickness (see Figure 4). The vortex is centred at approximately one quarter of the local boundary layer height (see Figure 11) and thus the imposition of the upper boundary conditions did neither suppress nor enhance the resulting vortex.

The highest and lowest level of flow field enhancement downstream of the AJVG was always achieved by two particular groups of pitch and skew angle configurations. The group of $30°/75°$ and $30°/60°$ enhanced most the flow field whereas the group of $30°/30°$ and $45°/30°$ generated the lowest enhancement. The vertical and the cross-stream velocity profiles (see Figures 18 and 19), the cross-stream vorticity (see Figure 24) and the wall shear stress (see Figure 26) showed exactly this behaviour. The highest magnitudes were achieved for the first group of $30°/75°$ and $30°/60°$ and lowest magnitudes for the second group of $30°/30°$ and $45°/30°$. Careful inspection of the circulation decay profiles (see Figure 20) shows also clearly that high values of skew angles, i.e. $\phi = 60°$, $\phi = 75°$ and rather a pitch angle of $\theta = 30°$ than $\theta = 45°$ are more favourite to increase substantially the level of circulation.

The initial level of circulation (see Figure 20) was increased by a factor of approximately 2.8 by altering the pitch/skew angles from $45°/30°$ to $30°/75°$. Changing the angle configuration again from $45°/30°$ to $30°/75°$ increased the level of initial peak vorticity (see Figure 21) by a factor of approximately 1.3. By altering the angle configuration from $45°/30°$ to $30°/75°$, the cross-stream movement (see Figure 22) increased proportional to that of the increase of peak vorticity. The cross-stream positions of the vortex cores (see Figure 18) coincide with the behaviour of the vorticity paths. The vertical positions of the vortex cores (see Figures 19 and 23) seem to be relatively independent of the particular pitch and skew angle configuration. The general position of the vortex cores is at approximately one quarter of the undisturbed boundary layer thickness. Of course, this result is a function of the particular duct and AJVG configuration considered.

The maximum enhancement of the flow field was observed by adjusting the pitch angle to $30°$ and the skew angle to $75°$. This configuration exhibited the highest level of circulation, peak vorticity and increase of wall shear stress.

The sector model does represent more realistically the physical geometry and conditions of the duct than does the flat plate model. Hence, the sector model would predict the paths of vortices of any size or position without any restrictions caused by the upper boundary or the

surface geometry as in the case of the flat plate model. In order to investigate the maximum flow field enhancement eight different pitch and skew angle configurations were tested. As mentioned before the individual size of the vortices compared to the solution domain width is the reason why only small differences between co- and counter-rotating vortices could be observed. However, comparing the upwash and downwash boundaries of the co- and counter-rotating configurations of the vertical velocity profiles (see Figure 18) the difference between periodicity and symmetry could be clearly observed. If the computations had been continued further downstream, so that the vortices started to interact more with the boundaries, then it could be expected that the two numerical models would start to predict results that differed more obviously.

CONCLUSIONS

Two numerical models were used to analyse the flow field development in the vicinity of an AJVG array in an internal flow application of a straight circular duct. Both the local flat plate model and the local sector model described an array of co- and counter-rotating vortices issuing into the main flow. There were two main differences between these models. The first difference is that the circumferential curvature of the duct was reflected only by the sector model. The second difference is in the way in which the upper boundary conditions were defined. In the case of the sector model the upper boundary was coincident with the centre line of the duct thus symmetry conditions were applied. Conversely, the flat plate model comprised a fixed domain height of five times the local boundary layer thickness and a constant pressure boundary condition was imposed.

The results of both numerical models at a pitch/skew angle configuration of 45°/45° showed differences of only an order of magnitudes of approximately 7 to 2 per cent. Hence, the difference can be seen as insignificant. However, it is suggested that the reason for this result is caused by the fact that the vortex arrays are weak and close to the wall. Thus, neither the upper boundary condition nor the cross-stream curvature could cause any significant impact onto the development of the vortices. It is stressed that the results are for one particular duct and AJVG configuration. Obviously, the ratio of vortex size to duct diameter is a parameter that needs to be investigated. Further research is necessary to see if significant differences might occur by producing stronger, larger vortices which would lift off the surface more and which are more influenced by the upper and side boundaries.

The sector model reflected more closely the physical geometry of the AJVG array in the straight circular duct. Hence, this model was used to generate a range of eight different pitch and skew angle configurations of co- and counter-rotating vortices. The maximum level of flow field enhancement in terms of a significant increase of skin friction and levels of peak vorticity and circulation was achieved using a pitch and skew angle configuration 30°/75°. The angle configuration of 45°/30° predicted the lowest level of enhancement.

All predicted vortex cores were positioned at approximately one quarter of the undisturbed boundary layer height. Hence, the vertical vortex position seemed not to be depending on the actual pitch/skew angle configuration. Boundary layer control was achieved rather by redistributing momentum within the boundary layer than by mixing high momentum fluid of the free stream, i.e. outside the boundary layer, with low momentum fluid within the boundary layer.

NOMENCLATURE

h_s	Domain height
d_j	Air-jet diameter
k	Turbulent kinetic energy
l_j	Jet inlet tube length
l_s	Domain length
Re	$= \dfrac{\rho U_0 x}{\mu}$
u, v, w	Fluctuating velocity components x, y, z directions
U, V, W	Mean velocity in components the x, y, z directions
U_0	Free stream velocity component in streamwise direction
w	Width of the numerical model/the wind tunnel working section
X, Y, Z	Locations in an orthogonal coordinate system
x, y, z	Orthogonal coordinates
δ	Streamwise boundary layer thickness
ε	Dissipation rate
θ	Pitch angle with respect to the solid surface
μ	Dynamic molecular viscosity
ν	Kinematic molecular viscosity
ρ	Fluid density
ϕ	Skew angle with respect to the centre line

Subscripts

0	Solution domain inlet condition
j	Jet inlet condition
s	Solution inlet condition
t	Turbulent
VG	Centre of the airjet vortex generator orifice

ACKNOWLEDGEMENTS

The authors would like to acknowledge the support under DERA Bedford Contract No. ASF/26714.

REFERENCES

1. Wallis RA. The use of air-jets for boundary layer control. Aeronautical Research Council, Australia, Aero Note 110, 1952.
2. Wallis RA. A preliminary note on a modified type of air-jet for boundary layer control. Aeronautical Research Council, Australia, Current-Paper CP 513, 1960.
3. Pearcey HH. Shock induced separation and its prevention. *Boundary Layer & Flow Control*, vol. 2. Pergamon: New York, 1961; 1170–1344.
4. Johnston JP, Nishi M. Vortex generator jets — means for flow separation control. *AIAA Journal* 1990; **28**(6): 989–994.
5. Compton DA, Johnston JP. Streamwise vortex production by pitched and skewed jets in a turbulent boundary layer. *AIAA Journal* 1992; **30**(3):640–647.
6. Zhang X. Computational analysis of co- and contra-rotating streamwise vortices in a turbulent boundary layer. *AIAA Paper No. 93-3035*, 1993a.

7. Henry FS, Pearcey HH. Numerical model of boundary-layer control using air-jet generated vortices. *AIAA Journal* 1994; **32**(12):2415–2425.
8. Akanni SD, Henry FS. Numerical calculations for air jet vortex generators in turbulent boundary layers. CEAS European Forum on High Lift & Separation Control, March, 1995, Bath, UK.
9. Oskam B, van der Berg B. Technical evaluation report on the Fluid Dynamics Panel symposium on improvement of aerodynamic performance through boundary layer control and high lift systems, AGARD, Neuilly sur Seine, France, p. 6, May, 1985.
10. Jacobi AM, Shah RK. Heat transfer surface enhancement through the use of longitudinal vortices: a review of recent progress. *Experimental Thermal and Fluid Science* 1995; **11**:295–309.
11. Gibb J, Anderson BH. Vortex flow control applied to aircraft intake ducts. CEAS European Forum on High Lift & Separation Control, March, 1995, Bath, UK.
12. Schlichting H. *Boundary Layer Theory*, 7th edn. McGraw Hill, 1979.
13. Henry FS, Reynolds AJ. Analytical solution of two gradient-diffusion models to turbulent couette flow. *Journal of Fluids Engineering* 1984; **106**:211–216.
14. Hinze JO. *Turbulence*. McGraw Hill, 1959.
15. CFX 4 User Manual. CFX 4 Release 4.1. CFDS, AEA Industrial Technology Harwell Lab., Oxfordshire, UK., October, 1995.
16. Küpper C. A study of the application of air-jet vortex generators to intake ducts. PhD Thesis, City University, 1999.
17. Küpper C, Henry FS. Numerical study of air-jet vortex generators in a turbulent boundary layer. *Applied Mathematical Modelling*: submitted.
18. Rodi W. Turbulence models and their application in hydraulics. Institut für Hydromechanik, Uni Karlsruhe, 1980.
19. Pauley WR, Eaton JK, Experimental study of the development of longitudinal vortex pairs embedded in a turbulent boundary layer. *AIAA Journal* 1988; **26**(7):816–823.

